Published in final edited form as:
Toxicol Mech Methods. 2008 ; 18(5): 385–398. doi:10.1080/15376510701611032.

Metabolomics in Lung Inflammation: A High Resolution ^{1}H NMR Study of Mice Exposed to Silica Dust

Jian Zhi Hu[*], **Donald N. Rommereim**, **Kevin R. Minard**, **Angie Woodstock**, **Bruce J. Harrer**, and **Robert A. Wind**
Pacific Northwest National Laboratory, Richland, Washington

Richard P. Phipps and **Patricia J. Sime**[*]
University of Rochester, School of Medicine and Dentistry, Rochester, NY 14642

Abstract

Here we report the first ^{1}H NMR metabolomics studies on excised lungs and bronchoalveolar lavage fluid (BALF) from mice exposed to crystalline silica. High resolution ^{1}H NMR metabolic profiling on intact excised lungs was performed using slow magic angle sample spinning (slow-MAS) ^{1}H PASS (phase altered spinning sidebands) at a sample spinning rate of 80 Hz. Metabolic profiling on BALF was completed using fast magic angle spinning at 2kHz. Major findings are that the relative concentrations of choline, phosphocholine (PC) and glycerophosphocholine(GPC) were statistically significantly increased in silica-exposed mice compared to sham controls, indicating an altered membrane choline phospholipids metabolism (MCPM). The relative concentrations of glycogen/glucose, lactate and creatine were also statistically significantly increased in mice exposed to silica dust, suggesting that cellular energy pathways were affected by silica dust. Elevated levels of glycine, lysine, glutamate, proline and 4-hydroxyproline were also increased in exposed mice, suggesting the activation of a collagen pathway. Furthermore, metabolic profiles in mice exposed to silica dust were found to be spatially heterogeneous, in consistent with regional inflammation revealed by *in vivo* magnetic resonance imaging (MRI).

Keywords

^{1}H NMR; MAS; metabolomics; metabolite; molecular pathways; MRI; inflammation

Introduction

Silicosis is a well-known occupational disease induced by inhalation of silica dust. Its incidence is greatly increased in industrial operations by mechanization and the use of sand blasting, drilling, pulverizing, cutting, grinding tools and other pneumatic equipment. Exposure to silica can generally contribute to a variety of diseases such as acute silicosis, pulmonary tuberculosis, interstitial fibrosis, industrial bronchitis, small air way disease, emphysema, rheumatoid complication, vascular disease, glomerulonephritis, immunologic reactions and cancer (Ding *et al*, 2002). Crystalline silica is highly toxic to the lung and is a recognized carcinogen. The mechanisms of silica injury have been the subject of extensive investigations during the last several decades and have been reviewed extensively by Ding *et al* (2002) and Knaapen *et al* (2004).

To whom correspondence should be addressed. Jianzhi.Hu@pnl.gov; Phone: (509) 376-9631; Fax: (509) 376-2303; Patricia_Sime@URMC.Rochester.edu.

Although the mechanisms for silica toxicity are not well-understood, it is widely recognized that oxidative stress plays a critical role (Knaapen *et al* 2004). Silica particles, for example, can directly generate oxidants such as silicon-based free radicals (SiO•, SiOO•) and hydroxyl radicals (•OH) from the Si-OH groups on the silica surface. Generally, this occurs through the so-called acellular process and its importance is mostly determined by the physico-chemical characteristics of the particle surface (Shi *et al* 1989, 1994, 1995, 1998 and Vallyathan *et al* 1992, 1998). Silica particles have also been found capable of inducing cellular oxidants via a variety of other mechanisms, including particle-related mitochondrial activation or NAD(p)H-oxidase enzymes (Deshpande *et al* 2002, Driscoll et al 2001, Li *et al* 2003, Shukla *et al* 2000 and Voelkel *et al* 2003) and inflammation-induced pathways (Schins 2002, Carter *et al* 2001, Porter *et al* 2002).

Generally, most oxidants can be categorized as either reactive oxygen species (ROS) or reactive nitrogen species (ROS). Both can be generated either by acellular or cellular processes. The most significant cellular ROS/RON generating system in the lung is the pool of inflammatory phagocytes (Knaapen *et al* 2004). Genotoxicity is caused by oxidant-induced DNA damage either by oxidative modification of DNA bases or induction of DNA single-strand breaks. If DNA-repair and selective apoptosis fail, mutagenesis occurs that ultimately leads to the development of cancer (Knaapen *et al* 2004).

Although abundant evidence suggests that ROS/RON mediate particle-induced genotoxicity and mutagenesis, little is known about the molecular pathways and networks that ultimately lead to neoplastic changes. It is well-known that alterations in DNA, RNA and enzymes (proteins) are associated with changes in the metabolic profiles. Metabolites are chemical compounds that participate as reactants, intermediates, or byproducts in a cellular metabolic pathway, and include carbon compounds with a molecular weight typically in the range 100-1000. Any insult should result in disturbances in the ratios and concentrations of endogenous metabolites, either by direct chemical reaction or by binding to key enzymes or nucleic acids that control metabolism. Therefore, metabolomics, defined as a comprehensive and quantitative analysis of all metabolites in a biological system, or alternatively, the global analysis of small molecule metabolites and metabolic patterns (Oliver 2001, Nicholson 1999, Sinha 2005) will be an important new tool in elucidating the molecular mechanisms in the progression of silicosis. Moreover, like DNA and protein enzymes, metabolic changes are the earliest cellular response to environmental or physiological changes. Metabolomics, although in its infancy, has already proven capable of detecting and diagnosing a disease and evaluating the efficacy of therapy at an early stage (Bollard *et al* 2005, Lindon *et al* 2003, Nicholson et al 1989, Reo 2002, Williams *et al* 2005). Therefore, it is highly likely that metabolomics will provide valuable insight into biological pathways and networks in silicosis.

Nuclear Magnetic Resonance (NMR) spectroscopy is a quantitative, non-destructive method that requires little or no sample preparation, and is one of the leading analytical tools for metabolomic research (Coen *et al* 2003, Dunn *et al* 2005, Griffin 2004, Holmes *et al* 1994, Lindon *et al* 2000, 2001a, 2001b, 2003, 2004 and Waters *et al* 2001). ^{1}H NMR is especially attractive because protons are present in virtually all metabolites and its NMR sensitivity is the highest among all the NMR observable nuclei. Also NMR chemical shifts are generally reproducible. This enables the simultaneous identification and monitoring of a wide range of low molecular weight metabolites, thus providing a biochemical fingerprint of an organism "without prejudice". However, in biological samples such as excised tissues and organs, cells attached to solid surfaces, and localized areas inside a live animal, the line width of the ^{1}H spectrum obtained from a static sample is broadened primarily by the variation in the bulk magnetic susceptibility present in intact cells and tissues. Other line broadening mechanisms include the residual chemical shift anisotropy interaction and the residual dipolar interaction among the abundant protons (Adebodun and Post 1993, Weybright *et al* 1998). This results in

an increase in overlapping spectral lines from different metabolites (Kreis R. 1997), which hampers analysis of the spectrum and limits the information that can be obtained by ^{1}H NMR.

In principle, the magnetic susceptibility, the residual chemical shift anisotropy and the residual dipolar interactions-induced line broadenings can be averaged to zero by the technique of magic angle spinning (MAS). In MAS, the sample is rotated about an axis at an angle of 54°44′ relative to the external magnetic field (Andrew and Eades 1959, Garroway 1982). High-resolution ^{1}H MAS spectroscopy at a spinning rate from several kHz to more than 10 kHz, i.e., the so-called fast-MAS, has been used to study metabolites in tissues and cells with notable success (Weybright *et al* 1998, Cheng et al 1997, Millis et al 1997, Garrod et al 1999, Bollard et al 2000, Garrod et al 2001, Chen J 2001). However, the large centrifugal force associated with these spinning rates destroys the tissue structure and even some of the cells (Weybright *et al* 1998), which makes the method unusable for applications where non-destructive detection is required. Furthermore at a fast sample spinning rate, it is difficult to keep all the fluids inside the MAS rotor without fluid leakage, making fast-MAS a demanding experiment.

Recently, we developed new so-called slow-MAS (magic angle spinning) NMR techniques (Bertram *et al* 2004, Hu *et al* 2002a, 2002b, 2003, 2004, 2006a, 2006b, Wind *et al* 2001, 2003a, 2003b, 2003c, 2004, 2005a, 2005b, 2006a, 2006b, 2006c) that significantly enhance the spectral information in biofluids, intact excised tissues, organs and live small animals (mice). Our slow-MAS NMR techniques were developed based on existing solid state NMR techniques, i.e., the phase altered spinning sidebands (PASS) (Antzutkin *et al* 1995) and the phase corrected magic angle turning (PHORMAT) (Hu *et al* 1995) experiments. With ^{1}H PASS, a sample spinning rate as low as 30Hz can be utilized, permitting non-destructive high resolution ^{1}H NMR metabolic profiling in cells, cells attached to solid surfaces, excised tissues and organs (Wind *et al* 2001, Hu *et al* 2004, 2006a, Wind and Hu 2006c). With ^{1}H PHORMAT, a sample spinning rate as low as 1Hz can be utilized, allowing *in vivo* high resolution ^{1}H NMR metabolic profiling in a small live animal such as a mouse. Recently, a localized ^{1}H PHORMAT experiment, namely the LOCMAT experiment, was developed in our laboratory, permitting high resolution ^{1}H metabolic profiling in an arbitrarily localized volume inside a live small animal (Hu *et al* 2002a, Wind *et al* 2003a, 2005b, 2006b and 2006c). Both ^{1}H PASS and ^{1}H PHORMAT are two dimensional NMR experiments, in which a high resolution ^{1}H NMR spectrum free from the magnetic susceptibility, the residual chemical shift anisotropy and residual dipolar interaction induced line broadening, is obtained. However, ^{1}H PASS offers superior sensitivity compared to ^{1}H PHORMAT and is the method of choice for non-destructive metabolic profiling in cells and excised tissues. It is also the method of choice for replacing fast-MAS. This is because it is easier to perform a PASS experiment than fast-MAS, as it is easy to keep all the fluids inside a slow-spinning MAS sample rotor without fluid leakage.

In this paper, the first NMR metabolomics study of mice exposed to crystalline silica dust is reported. ^{1}H PASS was used for metabolic profiling of excised intact lungs and ^{1}H fast-MAS using a special liquid-tight sample cell was employed for the analysis of bronchoalveolar lavage fluid (BALF). Results are discussed to gain insights into the molecular pathways and networks involved in lung inflammation and fibrosis.

Experimental

Animals and Sample preparation

Crystalline silica dust (with mean particle size < 5μm in diameter) (U.S. Silica Company, Berkeley Springs, WV) was chosen as a model airborne agent to introduce inflammation in the lungs of mice. This was accomplished using a well-established procedure based on intratracheal instillation (Dethloff et al 1986a, 1986b, Miller and Hook 1988, Driscoll *et al*

2000). Though intratracheal instillation is invasive, the results are easily controllable, reproducible and efficient (Driscoll *et al* 2000).

Preparation of silica (SiO_2)—The silica dusts were treated by boiling 30g of silica in 1 liter of 1.0M-HCl to remove any possible Fe_2O_3, which is known to contaminate the dust (Dethloff et al 1986a). The silica was then washed 4 times with deionized water to remove the acid and chloride. The preparation was dried in an oven at 100°C. Prepared silica was sterilized by dry heat (200°C, 2h) and diluted to the appropriate concentration with sterile 0.9% NaCl. Suspensions of known concentrations of SiO_2 for intratracheal instillation were sonicated for 10 minutes before use.

Dosing of animals—Mice were anaesthetized by inhalation of isoflurane. Isoflurane was administered as 2% isoflurane vapor in oxygen, using a vaporizer, host cage, and flexible rebreather (nose cone breathing apparatus) supplied by EZ-Anesthesia (Euthanex Corp., Palmer, PA). The vaporizer and host cage were placed in a Biosafety Level-1 (BSL-1) cabinet, which was exhausted outside. The rebreather and surgical bed were also placed inside the BSL-1 cabinet for the convenience of the surgeon. The method of trans-tracheal instillation (Thrall *et al* 1978) was employed, whereby the trachea was exposed surgically on the ventral side of the neck, and a needle was inserted through the tracheal wall into the lumen just below the larynx. After instillation, the cut was surgically closed. Female C57BL/6 mice (6-8 weeks old) were used. Mice were purchased from Jackson Laboratories and housed in Pacific Northwest National Laboratory's Animal Facilities that are fully accredited by the American Association of Laboratory Animal Medicine and are in compliance with federal statute and NIH policy. Females were selected for this study because males are prone to fighting when housed in groups, especially upon entering adulthood (Gridley *et al* 2006). Wounds from such fights can become infected, which may confound interpretation of the experimental data and increasing animal-to-animal variability.

Sample Collection—A total of 24 mice were used and were randomly separated into 2 groups, consisting of sham controlled (n=12), and silica-exposed (n=12) groups. Intratracheal instillation was performed at day 0 on both groups. The mice in the control group were instilled with 40μl of saline while the silica exposed mice were instilled with silica suspension at a dose of 5mg/mouse suspended in 40μl of saline. On day 7 and 4 months post exposure, 4 mice were sacrificed from each group with CO_2 asphyxiation, and samples collected, including lungs and bronchoalveolar lavage fluids (BALF). All the samples were stored immediately after collection at −80°C until use. The sample size, n=4, was chosen to deal with normal biological variation. BALF was collected by quickly excising the lungs with their tracheae intact. After removing extraneous tissue, the trachea was cannulated and the lungs filled to capacity with a total of 1.0 ml ice-cold 0.9% saline. Lavage effluents were then collected and refilled into the lungs to repeat the lavarge process. This procedure was repeated three times, resulting in approximately 0.8ml of lavage fluid for each mouse. On day 14 post exposure, 4 mice from each group were subjected to magnetic resonance imaging (MRI) test. All animal work was approved by the Institutional Animal Care and Use Committee (IACUC) at the Pacific Northwest National Laboratory.

NMR Experiments

The ^{1}H NMR metabolic profiling experiments were performed on a Varian-Chemagnetics 300 MHz Infinity spectrometer, with a proton Larmor frequency of 299.982 MHz. A standard Chemagnetics CP/MAS probe with a 7.5-mm pencil type spinner system was used. Two sample spinning rates, i.e., slow and fast, were used depending on the type of experiments performed. A slow sample spinning rate of 80Hz was used for metabolic profiling on excised intact lungs using the ^{1}H PASS technique (Wind *et al* 2001, Hu *et al* 2004), while a fast sample spinning

rate of 2kHz (fast-MAS) was used for metabolic profiling of BALF. In order to spin at low frequencies, i.e., 80Hz, the rotor was equipped with a flat drive tip (i.e. it did not contain grooves, which are normally used to drive the rotor) and an airflow restriction was utilized in the driver channel. The spinning rate was controlled using a commercial Chemagnetics MAS speed controller under the automated control mode. By marking the rotor at three evenly spaced intervals, the frequency stability is better than ±0.3 Hz at spin rates of 80Hz. By removing the air restrictor and using normal spinning tips, normal sample spinning rate of more than 2kHz was conveniently reached.

In vivo ^{1}H MRI experiments were performed at 85 MHz using a UnityPlus imaging console (Varian, Palo Alto, CA) and a 2T horizontal bore magnet (Oxford Instruments, Oxford, UK) equipped with self-shielded gradients (Resonance Research Inc., Billerica, MA). Prior to imaging, all mice were anesthetized with a mixture of 0.3 ml Xylazine at a concentration of 20 mg/ml and 1.0 ml of Ketamine at a concentration of 100 mg/ml. The cocktail mixture was then administered by intraperitoneal injection at 1.4 μl/g mouse body weight. The anesthesia lasted for 1.5–2.5 hr (Wind et al 2006). Mice were then placed inside a custom-built radio-frequency (RF) coil that was used to excite and receive the NMR signal during image collection. The RF coil had an inner diameter of 5.4 cm and was based on the Alderman-Grant design (Alderman et al 1979).

During imaging normal body temperature was maintained by blowing warm air into the magnet bore. To visualize lung anatomy, raw image data were collected on a 256×256×64 matrix using a 3D gradient-echo sequence with a 1 msec echo-time, a repetition time of 31 msec, a 10° flip angle, and 2 averages. Each 3D data set required 17 minutes to collect and showed a cubic field of view that was 6.4 cm on a side after Fourier reconstruction was performed on a zero-filled matrix that was 512×512×128. Use of zero filling provided linearly interpolated images that were then stored as 128 contiguous slices that were 500 microns thick and characterized by an interpolated resolution of 125 microns.

Experimental Results

Spectral resolution comparison between static ^{1}H NMR, ^{1}H PASS and ^{1}H fast-MAS on excised lung

Figure 1 compares the spectral resolution obtained by traditional ^{1}H NMR on a static sample, ^{1}H PASS at 80Hz and fast-MAS at a sample spinning rate of 2kHz using a sample consisting of an entire intact left lung lobe from a silica exposed C57BL/6 mouse. The static ^{1}H NMR obtained by conventional water suppressed NMR (Fig. 1a) shows only a few broad peaks arising from lipids (0.8, 1.28ppm) and total choline (3.2ppm). The line broadening is caused mainly by the magnetic susceptibility variation inside the intact excised lung in addition to a less significant line broadening from the probe housing. The ^{1}H PASS spectrum in Fig. 1b along with its 3.2 times vertically expanded spectrum show significantly enhanced spectral resolution. The enhanced spectral resolution allows many metabolites to be observed and their assignments are depicted in Fig. 1. For example, lactate, alanine, glutamate, creatine, lysine, as well as choline, phosphocholine (PC) and glycerophosphocholine (GPC) that are not resolved in the static spectrum of Fig. 1a are all clearly separated in the PASS spectrum. Fig. 1c gives the fast-MAS spectrum obtained on the same sample. Fig. 1c was acquired immediately after the PASS experiment at a sample spinning arte of 2kHz using exactly the same experimental conditions as those of PASS except the shimming of the magnet was optimized using the strong H_2O signal from the sample at both spinning rates, separately. It is obvious that the 80Hz PASS produces better spectral resolution than fast-MAS using the identical experimental set-up. For example, many fine structures are obtained in the PASS spectrum but are obscured in the fast-MAS spectrum. This is because in the fast-MAS experiment, the tissue is redistributed against the inner rotor wall by the high centrifugal force,

forming a hollow cylinder of tissue mass inside the rotor and an extra magnetic susceptibility gradient from the rotor axis towards the surface of the rotor. Such an extra susceptibility gradient is very difficult to shim out with the existing spectrometer shim set. This results in a poor spectral resolution compared to ^{1}H PASS, where the tissue is more homogeneously distributed inside the rotor. The centrifugal force F_c is given by $F_c = \omega^2 r$, where r is the distance between the point of interest and the rotor axis and $\omega = 2\pi f$, f is the spinning frequency in Hz. Given that the inner diameter of the sample rotor of 6mm and a spinning rate of 80Hz, the maximum centrifugal force is only about 90 times the gravitational force, which is safe for maintaining the integrity of the tissues. In fact, a sample spinning rate of 600Hz has been reported capable of maintaining the tissue integrity of excised prostate tissue (Taylor *et al* 2003). However, at a sample spinning rate of 2kHz, the centrifugal force is as high as 5×10^4 the gravitational force. Fast-MAS applied at a sample spinning rate of 4kHz has been reported destructive to cells, causing significant cell lysis (Weybright *et al* 1998). Given the fact that it is much easier to load a sample for slow spinning experiment without fluid leakage, the ^{1}H PASS method is the preferred experiment for metabolic profiling on excised tissues.

^{1}H PASS metabolic profiling on excised intact lungs of control and silica exposed mice

The typical ^{1}H PASS spectra of excised lungs from both the silica exposed and sham-control C57BL/6 mice at 7 days and 4 months post treatment are given in Figure 2. In Fig. 2, for both the 7 day and the 4 month treatments, two sets of spectra of lungs from two different mice in each group are shown to illustrate the possible biological variations. Also in the plots, all the spectra are scaled to the intensity of lipid peak at about 1.28 ppm, i.e., the intensity of the lipid peak is plotted to the same height to facilitate the comparison among/between the various spectra.

The following observations can be made from Figure 2. Biological variations are clearly noticed in the sham control mice that were sacrificed 4 months post saline instillation, i.e., Figs. 2f and 2h, where the relative spectral intensities of total choline (choline, PC and GPC) and the glycogen/glucose in Fig. 2h are apparently higher than those in Fig. 2f. Also the intensity of the total choline in Fig. 2g is apparently higher than that in Fig. 2e for the silica exposed mice. Despite the biological variations, the intensities of total choline and the intensities of glycogen/glucose peaks are significantly increased in the spectra of lungs from mice exposed to silica dust by a factor of 6 to 10 (Figs. 2e and 2g) relative to those of sham-controls (Figs. 2f and 2h). Similar results are obtained from mice 7 days post treatments, where the biological variations in the silica exposed mice, Figs. 2a and 2c, are relatively larger that that of 4 months post treatment, Figs. 2e and 2g. This is probably due to the fact that the intratracheal instillation is far from a non-invasive procedure and the recovery would depend on the details of the procedure as applied to each animal that would never be the same. Furthermore, the exact amount of silica delivered to the lung depends on the details of implementation of the procedure and may not be the same as well. Also the mouse in Fig. 2a was one week younger than that of Fig. 2c at the time of instillation, which might also contribute to the observed variation. Nevertheless, the intensities of total choline peak as well as the intensities of glycogen/glucose in the lungs of mice treated with 5 mg silica dust 7 days post exposure, Figs. 2a and 2c, are significantly higher than those of sham-controls, Figs. 2b and 2d. Even if one compares Fig. 2a, the least elevated choline intensity from the silica exposed mouse, and Fig. 2d, the highest choline intensity from the sham-control mice, the conclusion is still true, i.e., the intensities of choline, PC, GPC, glycogen/glucose are significantly enhanced, by at least two fold, in the lungs of mice exposed to silica dust relative to sham-controls. In addition to the choline, PC, GPC and glycogen/glucose, a careful examination reveals that the relative spectral intensities corresponding to lactate, glutamate, creatine and lysine are also increased significantly in silica exposed mice in relative to those of sham-controls.

To highlight the low intensity spectral features, the corresponding spectra in Figure 2 (c), (d), (g) and (h) were vertically expanded 4 times and the resulting spectra between chemical shift values of 2.0 and 3.0ppm are plotted in Figure 3. In Figure 3, the locations for the peaks of 4-hydroxyproline are highlighted. It appears that the relative concentration of 4-hydroxyproline is also enhanced in mice exposed to silica compared with that from the control mice at both 7 days and 4 months post treatment.

Statistical Analysis

The statistical significance between the metabolites of the excised lungs from the controls and the silica exposed C57BL/6 mice was determined using the "Student's *t* test" (Steel RGD and Torrie JH 1960). Before the statistical analysis, the data were processed in the following way. In each spectrum the integral intensity for the lipid $(CH_2)_n$ peak centered at about 1.28ppm was normalized to 1.0. The corresponding integral range was approximately from 1.22 to 1.3ppm for the lipid peak. The relative integrated intensities for all the other peaks were then determined based on the chemical shift ranges, i.e., methyl peak is integrated from about 0.8 to 1.0ppm, lacate from about 1.30 to 1.36ppm, alanine from about 1.44 to 1.51ppm, proline and lipid CH=CH-C$\mathbf{H}_2$-CH_2 from about 1.95 to 2.21, 4-hydroxyproline from about 2.10 to 2.20 ppm, glutamic acid from about 2.31 to 2.42ppm, lysine from about 2.91 to 3.01ppm, creatine from about 3.01 to 3.08 ppm, total choline (choline +PC +GPC) from about 3.13 to 3.36ppm, glycogen/glucose from about 3.36 to 4.0ppm, and glycine from about 3.536 to 3.577ppm, respectively. These relative integral intensities were then subject to the "Student *t* tests" and the results for the 7 days and the 4 months post treatments are summarized in Table 1.

It follows from Table 1 that at day 7 post treatment, the relative levels of CH_3, lactate, alanine, proline, 4-hydroxyproline, glutamic acid, lysine, creatine, total choline, glycogen/glucose and glycine are statistically significantly increased with $p \leq 0.03$. Similar results are found for the relative levels of total choline, glycogen/glucose and 4-hydroxyproline at 4-month post treatment. However, the level of CH_3 is not significantly different between the silica exposed mice and the control mice at this time point, i.e., 4-month post treatment.

Spatial heterogeneity of metabolites

Figure 4 shows the ^{1}H PASS spectra acquired at a sample spinning rate of 80Hz on two spatially different sections in the lung. Fig. 4a corresponds to tissue from major airways. Fig. 4b corresponds to distal lung tissues. It follows from Fig. 4 that the levels of lactate, alanine, glutamate, creatine, PC and GPC are significantly increased in Fig. 4a over those in Fig. 4b. These results indicate that the lung sections close to the trachea and close to the bronchi are more diseased than the peripheral locations. This is apparently a natural consequence of the intratracheal instillation method used because silica dust preferentially deposits in locations that are close to the trachea. The spatial heterogeneity of lung inflammation is further supported by *in vivo* magnetic resonance imaging results that are presented in Figure 5 and discussed in the next section. Importantly, the results obtained from this study also serve as a self controlled study where the biological variation between different mice is avoided. The significantly elevated PC, GPC, lactate, alanine, glutamate and creatine levels in tissues of major airways (Fig. 4a) in relative to those of distal tissues (Fig. 4b) of the same mouse strongly support the findings obtained from Fig. 2 since the tissues of the major airways are more diseased.

Monitoring pulmonary inflammation caused by silica dust using *in vivo* magnetic resonance imaging (MRI)

When inflammation occurs in the lung, water accumulates inside the alveolar space and inside the cells. We found that the lung weight doubled in mice 14 days after silica instillation. A similar study in rats concluded that water content accounts for more than 80 percent of the

increase in lung weight (Dethloff *et al* 1986). This water accumulation can be detected by MRI as illustrated in Figure 5. Figs. 5A and 5B show MR images of a control mouse (A) and a treated mouse 14 days after it was instilled with 5 mg silica dust (B). Both mice weighed less than 20 grams and each was imaged with transverse slices oriented approximately perpendicular to the body axis. Slice 1 in each series is located at the top of the lung near the trachea, and slice 14 is located down near the liver. To facilitate comparisons, all data were acquired and displayed under identical conditions. Comparing slice 5 to 11 shows that significant fluid accumulation and spatial heterogeneity is associated with silica dust exposure. This is illustrated by the much higher signal intensity from elevated water content around the main airways observed in Fig.5. B8 (compare to panel Fig. 5. A8 in control mouse). To quantify intensity differences, each lung was manually segmenting from 3D image data and signal in each slice was summed. Measurements from 3 controls and 3 exposed mice gave 216±2 and 394±50 respectively. This This statistically significant difference ($p=0.007$) is close to the factor of two measured in lung weight and is further evidence that weight changes are largely attributable to alterations in water content. These results indicate that MRI might serve as a convenient tool for observing early fluid accumulation that is associated with silica-induced inflammation. Because MRI is noninvasive, it can potentially be used at different intervals throughout a study to monitor changes in fluid accumulation that could correlate with inflammatory infiltrates, fibrosis, or ultimately the development of neoplastic masses.

^{1}H NMR metabolic profiling in BALF

BALF is obtained by washing the inside of the lung with saline, and it contains both extracellular and intracellular metabolites. The extracellular metabolites are those small molecules soluble in saline while intracellular metabolites are those inside of cells, such as the macrophages that have been lavaged off the alveolar surfaces. Not surprisingly, we found that the overall metabolite concentration in BALF is much lower than that in the other body fluids such as urine and blood. Thus, relatively larger sample volumes need to be used to obtain sufficient sensitivity. Even though slow-MAS ^{1}H PASS permits high resolution NMR metabolic profiling of biofluids such as urine and plasma with volume as small as 2.5μl (Hu *et al* 2006b), we found that ^{1}H PASS applied at a sample spinning rate of 80Hz does not work on large fluid samples such as BALF, where the viscosity is low. This is because fluids of large quantity with low viscosity do not rotate at the same spinning rate as the rotor, i.e., there is a speed gradient within the fluids while a uniform speed for the entire sample is required for PASS to work appropriately. Hence, in this case, due to its high sensitivity, fast MAS is the preferred method for removing the rotor-induced susceptibility broadening, as well as the intracellular line broadening. To this end, a novel liquid-tight sample cell, shown in Figure 6g, was developed for high resolution ^{1}H NMR metabolic profiling in fluids using magic angle spinning at spinning rate of 2kHz or more. The sample cell (Fig. 6g) is essentially 100% liquid-tight and fits into our 7.05T Varian-Chemagnetics 7.5mm MAS rotor. The sample volume of the cell can be conveniently adjusted from 50 to 120 micro-liters. Using this cell, we have performed experiments (results not shown) with 80 μl sample of 50 μM (micro-Molar) lactate in regular distilled water and found that reasonable S/N of the lactate methyl can be obtained in about 2 hour data acquisition at 7.05T field. A significant advantage of MAS over traditional high resolution solution NMR is that raw lavage fluid containing cells can be studied. Cells are preferably removed in a standard high resolution solution NMR experiment in order to obtain high spectral resolution. As such the intracellular metabolites are not detected by standard NMR. In the MAS experiment with the liquid-tight cell, quantification of the BALF spectrum has been achieved by sealing a tiny drop of silica sealant into a separate compartment of the rotor that is located very close to but physically separated from the sample chamber (see label “g5” in Fig.6g). The external standard permanently resides inside the rotor, so that the same external standard can be used on samples from different mice. Moreover, this standard is also used as a chemical shift reference. Typical results on the BALF samples of both sham

control and silica treated mice 7 days post exposure are summarized in Figure 6. It should be pointed out that the BALF samples used to acquire the spectra in Figs. 6a, 6b, 6c and 6d were obtained from the corresponding mice in Figs. 2a, 2b, 2c and 2d, respectively.

The peak intensities for the various metabolite peaks relative to the permanent external standard (defined as 1.0) indicated by "*" in Fig. 6 are listed in Table 2, where the all the peak intensities were measured from the root of the individual peak, i.e., the broad line features were subtracted.

The following results are from Fig. 6 and Table 2. (i) Glycerophosphocholine (GPC) labeled as "7" in the spectra is increased significantly in silica exposed mice over sham control mice. (ii) Lactate (peak "1"), acetate (peak "3"), creatine (peak "4") and alanine (peak "2") are significantly increased in silica exposed mice over sham control mice. This is consistent with an acute inflammatory process that damages lung cells, releasing lactate and creatine (Cramer *et al* 2003,Haji-Michael *et al* 1999). The significantly increased concentration in GPC is derived from damaged cell membranes, which complements the findings obtained from direct metabolic profiling on excised lung tissues (Fig. 2).

Discussion

Our experimental results from metabolic profiling on BALF and excised lungs clearly indicate that the relative levels of choline, PC, GPC, glycogen/glucose, lactate, acetate, glutamate, lysine and creatine are significantly increased in mice exposed to silica dust.

Phosphocholine is an important intermediate product in the membrane choline phospholipid metabolism (MCPM) (Figure 7) where PC, GPC are synthesized and hydrolyzed (Aboagye EO et al, 1999). Generally, phosphatidylcholine is the most abundant phospholipid in biological membranes and together with other phospholipids, such as phosphatidylethanolamine and neutral lipids, form the characteristic bilayer structure of cells and regulate membrane integrity (Mountford CE, et al 1988). Prior studies have shown that elevated phosphocholine or total choline levels are strongly associated with malignancy (Aboagye EO et al, 1999,Mackinnon WB, et al, 1997,Ruiz-Cabello J, et al, 1992). The significantly increased phospholipids and total choline levels indicate an altered membrane choline phospholipids metabolism, suggesting that instilled silica dust causes damage to the cell membrane.

The MCPM pathway (Figure 7) is networked with arachidonic acid metabolism (Figure 8) by phospholipase A2 (PLA_2) that hydrolyzes arachadonic acid and represents the rate limiting step in eicosanoid production. The precursor molecule, arachidonate, is a 20-carbon, polyunsaturated fatty acid and metabolites of arachidonic acid are termed eicosanoids. PLA_2 is believed to be the primary enzyme responsible for release of arachidonate from cell membrane phospholipids. PLA_2 exists in both secretory and intracellular forms. Regulation of intracellular forms of PLA_2 is important for stimulating arachidonic acid release during inflammatory reactions (Spurney and Coffman 1995). Figure 8 indicates that the prostaglandin (PG) synthesis pathway begins with the release of arachidonic acid from phospholipid membranes by the action of PLA_2. Arachidonic acid is the substrate for two distinct enzymatic pathways, cyclooxygenases (Cox-1, Cox-2) and 5-lipoxygenase. The end-products of the 5-lipoxygenase pathway are leukotrienes, whereas the Cox pathway gives rise to prostaglandins and thromboxanes. The Cox enzymes convert arachidonic acid to the prostaglandin PGH_2, which is further processed to individual PGs by specific PG synthases (Spurney and Coffman 1995). In previous studies, we have investigated the role of the fibroblast as a sentinel cell capable of modulating immune-inflammatory reactions (Smith *et al* 1997). In these experiments, primary human lung fibroblasts were treated with silica for 24 hours, and Cox-2 expression was evaluated by western blot and immunocytochemistry. We found that crystalline

silica induced Cox-2 expression in a dose-dependent manner (O'Reilly *et al* 2005), and the arachidonic acid metabolism pathway was altered. Since both PGs and leukotrienes are relatively small molecules, a metabolomics study would yield valuable information on this pathway, which will be a focus of our future investigations. It is expected that the metabolites in arachidonic acid metabolism have relatively low concentrations compared to those of MCPM and therefore may be difficult to detect by NMR based metabolomics on tissue samples. Mass spectrometry based metabolomics, e.g., LC-MS, offers much higher sensitivity than NMR. Although it is destructive and requires an extra step of sample extraction, it would be the method of choice for this investigation (Shen *et al* 2005).

The increased levels of glycogen/glucose, lactate and creatine indicate alternations of the cellular energy pathways (Jue T. 2005, Pollard and Earnshaw 2004) (see Figure 9). It follows from Fig. 9 that glycogen, lactate and creatine are end products in the cellular energy pathway and thus observed by our *ex vivo* metabolic profiling on excised intact lung tissues. Since this pathway is directly related to lipid utilization, we hypothesize that lipid breakdown is somehow linked to the MCPM pathway. The cellular energy pathways in muscle contraction has been a subject of intensive research (Jue T. 2005). It may be reasonable to view lung tissue as a special muscle due to its unique dynamics associated with breathing cycles. Lungs need energy to contract and expand, so it would not be surprising that metabolites associated with the cellular energy pathway are altered as a result of lung inflammation due to silica dust.

The levels of glycine, lysine, glutamate, proline and 4-hydroxyproline were significantly increased in the lungs of silica exposed mice compared to controls. Since glycine, lysine, glutamate, proline and 4-hydroxyproline are collagen metabolites (Schiller *et al* 2001, Keshari *et al* 2005), these results indicate the activation of the collagen pathway in mice exposed to silica dust. Hydroxyproline is produced by hydroxylation of the amino acid proline by prolyl hydroxylase. It is not directly coded for by DNA, however, and is hydroxylated after protein synthesis. Hydroxyproline is a major component of the protein collagen. Hydroxyproline and proline play key roles for collagen stability (Nelson and Cox 2005). They permit the sharp twisting of the collagen helix (Brinckmann et al 2005). It helps provide stability to the triple-helical structure of collagen by forming hydrogen bonds. Hydroxyproline is found in few proteins other than collagen. The only other mammalian protein which includes hydroxyproline is elastin (Ward and Courts 1977). For this reason, hydroxyproline content has been used as an indicator to determine collagen and/or gelatin amount. It is also known that myofibroblasts are key effector cells in scar formation including the generation of fibrotic lesions in lung fibrosis, and are prominent in tissues from patients with radiation-induced fibrosis and idiopathic pulmonary fibrosis (IPF) (Zhang *et al* 1994). Myofibroblast differentiation and proliferation and production of excess collagen and other extracellular matrix molecules are critical in the fibrogenic response (Sime *et al* 1997).

Conclusions

The recently developed slow-MAS ^{1}H PASS technique applied at a sample spinning rate of about 80Hz allows high resolution metabolic ^{1}H NMR profiling on excised intact lungs. Additionally, fast-MAS using a liquid-tight sample cell allows high resolution ^{1}H NMR metabolic profiling on raw BALF at a sample spinning rate of about 2kHz. Major findings from this investigation show that the relative concentrations of choline, phosphocholine (PC) and glycerophosphocholine (GPC) are statistically significantly increased in the lungs and BALF from silica exposed mice *versus* sham controls, suggesting an altered membrane choline phospholipids metabolism (MCPM) in lung inflammation. The relative concentrations of glycogen/glucose, lactate and creatine are also statistically significantly increased in mice exposed to silica dust, suggesting that the lung cellular energy pathways are also affected due to silica dust. Glycine, lysine, glutamate, proline and 4-hydroxyproline are statistically

significantly increased in mice exposed to silica dust, suggesting the activation of the collagen pathway, a process leading to lung scarring. Based on these findings, we suggest that MCPM, arachidonic acid metabolism, cellular energy pathway and collagen pathways are candidates for pathways that are altered in lung inflammation arising from inhaled silica dust. Furthermore, these pathways are internally networked to regulate lung inflammation and remodeling and are possible major pathways responsible for disease pathogenesis in silicosis. Additionally, metabolic profiles from the lungs of mice exposed to silica dust were found to be spatially heterogeneous, consistent with the inflammation revealed by *in vivo* magnetic resonance imaging (MRI) study.

Acknowledgments

This work was supported by the Pacific Northwest National Laboratory Directed Research and Development (LDRD) and Individual Research and Development (IR&D) projects. The research was performed in the Environmental Molecular Sciences Laboratory (a national scientific user facility sponsored by the Department of Energy's Office of Biological and Environmental Research) located at Pacific Northwest National Laboratory, and operated for DOE by Battelle. Dr. Phipps and Dr. Sime were supported by HL075432, ES01247, DE 011390 and an EPA-PM center.

References

Aboagye EO, Bhujwalla ZM. Malignant transformation alters membrane choline phospholipids metabolism of human mammary epithelial cells. Cancer Res 1999;59:80–84. [PubMed: 9892190]

Adebodun F, Post J. Bulk magnetic susceptibility induced line broadening in the ^{19}F NMR spectra of suspended leukemic cells. NMR Biomed 1993;6:125–129. [PubMed: 8499242]

Alderman DW, Grant DM. An efficient decoupler coil design which reduces heating in conductive samples in superconducting spectrometers. J. Magn. Reson 1979;36:47–451.

Andrew ER, Eades RG. Removal of dipolar broadening of NMR spectra of solids by specimen rotation. Nature 1959;183:1802.

Antzutkin ON, Shekar SC, Levitt MH. Two-dimensional sideband separation in magic-angle-spinning NMR. J. Magn. Reson 1995;A115:7–19.

Bertram HC, Hu JZ, Rommereim DN, Wind RA, Andersen HJ. Dynamic high-resolution ^{1}H and ^{31}P NMR spectroscopy and ^{1}H T_2 measurements in postmortem rabbit muscles using slow magic angle spinning. J. Agric. Food Chem 2004;52:2681–2688. [PubMed: 15113176]

Bollard ME, Garrod S, Holmes E, Lindon JC, Humpfer E, Spraul M, Nicholson JK. High-resolution ^{1}H and ^{1}H-^{13}C Magic Angle Spinning NMR Spectroscopy of Rat Liver. Magn. Reson. Med 2000;44:2901–207.

Bollard ME, Stanley EG, Lindon JC, Nicholson JK, Holmes E. NMR-based metabonomic approaches for evaluating physiological influences on biofluid composition. NMR in Biomedicine 2005;18:143–162. [PubMed: 15627238]

Brinckmann, J.; Notbohm, H.; Müller, PK. Collagen, Topics in Current Chemistry. Springer; Berlin: 2005. p. 247

Carter JD, Driscoll KE. The role of inflammation, oxidative stress, and proliferation in silica-induced lung disease: a species comparison. J. Env. Pathol. Toxicol Oncol 2001;20:33–43. [PubMed: 11570672]

Chen J, Enloe BM, Fletcher CD, Cory DG, Singer S. Biochemical analysis using high-resolution magic angle spinning NMR spectroscopy distinquishes lipoma-like well-differentiated liposarcoma from normal fat. J. Am. Chem. Soc 2001;123:9200–9201. [PubMed: 11552844]

Cheng LL, Ma MJ, Becerra L, Ptak T, Tracey I, Lackner A, Gonzalez RG. Quantitative neuropathology by high resolution magic angle spinning proton magnetic resonance spectroscopy. Proc. Natl. Acad. Sci. USA 1997;94:6408–6413. [PubMed: 9177231]

Coen M, Lenz EM, Nicholson JK, Wilson ID, Pognan F, Lindon JC. An integrated metabonomic investigation of acetaminophen toxicity in the mouse using NMR spectroscopy. Chem. Res. Toxicol 2003;16:295–303. [PubMed: 12641429]

Cramer T, Yamanishi Y, Clausen BE, Frorster I, Pawlinski R, Mackman N, Haase VH, Jaenisch R, Corr M, Nizet V, Firestein GS, Gerber HP, Ferrara N, Johnson RS. HIF-1α is essential for myeloid cell-mediated inflammation. Cell 2003;112:645–657. [PubMed: 12628185]

Deshpande A, Narayanan PK, Lehnert BE. Silica-induced generation of extracellular factor(s) increases reactive oxygen species in human bronchial epithelial cells. Toxicol. Sci 2002;67:275–283. [PubMed: 12011487]

Dethloff LA, Gilmore LB, Brody AR, Hook GE. Induction of intra- and extra-cellular phospholipids in the lungs of rats exposed to silica. Biochem. J 1986;233:111–118. [PubMed: 3006655]

Dethloff LA, Gilmore LB, Gladen BC, George G, Chhabra RS, Hook GE. Effects of silica on the composition of the pulmonary extracellular lining. Toxicol. Appl. Pharmacol 1986;84:66–83. [PubMed: 3012822]

Ding M, Chen F, Shi X, Yucesoy B, Mossman B, Vallyathan V. Disease caused by silica: mechanisms of injury and disease development. Int. Immunopharmacology 2002;2:173–182.

Driscoll KE, Costa DL, Hatch G, Henderson R, Oberdorster G, Salem H, Schlesinger RB. Intratracheal instillation as an exposue technique for evaluation of respiratory tract toxicity: Uses and Limitations. Toxicological Sciences 2000;55:24–35. [PubMed: 10788556]

Driscoll KE, Howard BW, Carter JM, Janssen YM, Mossman BT, Isfort RJ. Mitochondrial-derived oxidants and quartz activation of chemokine gene expression. Adv. Exp. Med. Biol 2001;500:489–496. [PubMed: 11764986]

Dunn WB, Ellis DI. Metabolomics: Current analytical platforms and methodologies. Trends in Analytical Chemistry 2005;24:285–294.

Fiehn O. Combining genomics, metabolome analysis, and biochemical modelling to understand metabolic networks. Comparative and Functional Genomics 2001;2:155–168. [PubMed: 18628911]

Garrod S, Humpfer E, Spraul M, Connor SC, Polley S, Connelly J, Lindon JC, Nicholson JK, Homes E. High-resolution magic angle spinning ^{1}H NMR spectroscopic studies on intact rat renal cortex and medulla. Magn. Reson. Med 1999;41:1108–1118. [PubMed: 10371442]

Garrod S, Humpher E, Connor SG, Connelly JC, Spraul M, Nicholson JK, Holmes E. High-resolution ^{1}H NMR and magic angle spinning NMR spectroscopic investigation of the biochemical effects of 2-bromoethanamine in intact renal and heptic tissue. Magn. Reson. Med 2001;45:781–790. [PubMed: 11323804]

Garroway AN. Magic-angle sample spinning of liquids. J. Magn. Reson 1982;49:168–171.

Griffin JL. Metabolic profiles to define the genome: can we hear the phenotypes? Phil. Trans. R. Soc. Lond. B 2004;359:857–871. [PubMed: 15306403]

Gridley DS, Dutta-Roy R, Andres ML, Nelson GA, Pecauta MJ. Acute Effects of Iron-Particle Radiation on Immunity. Part II: Leukocyte Activation, Cytokines and Adhesion. Radiation Research 2006;165:78–87. [PubMed: 16392965]

Haji-Michael PG, Ladriere L, Sener A, Vincent JL, Malaisse WJ. Leukocyte glycolysis and lactate output in animal sepsis and *ex vivo* human blood. Metabolism 1999;48:779–785. [PubMed: 10381154]

Holmes E, Foxall PJD, Nicholson JK, Neild GH, Brown SM, Beddell CR, Sweatman BC, Rahr E, Lindon JC, Spraul M, Neidig P. Automatic data reduction and pattern recognition methods for analysis of ^{1}H nuclear magnetic resonance spectra of human urine from normal and pathological states. Anal. Biochem 1994;220:284–296. [PubMed: 7978270]

Hu JZ, Wang W, Liu F, Solum MS, Alderman DW, Pugmire RJ, Grant DM. Magic-angle-turning experiments for measuring chemical–shift-tensor principal values in powdered solids. J Magn Reson A 1995;113:210–222.

Hu JZ, Rommerein DN, Wind RA. High resolution ^{1}H NMR spectroscopy in rat liver using magic angle turning at a 1 Hz spinning rate. Magn. Reson. Med 2002;47:829–836. [PubMed: 11979560]

Hu JZ, Wind RA. The evaluation of different slow-MAS techniques at low spinning rates in aqueous samples and in the presence of magnetic susceptibility gradient. J. Magn. Reson 2002;159:92–100. [PubMed: 12468309]

Hu JZ, Wind RA. Sensitivity-enhanced phase corrected ultra-slow magic angle turning using multiple-echo data acquisition. J. Magn. Reson 2003;163:149–162. [PubMed: 12852919]

Hu JZ, Wind RA, Mclean J, Gorby YA, Resch CT, Fredrickson JK. High-resolution ^{1}H NMR spectroscopy of metabolically active microordanisms using non-destructive magic angle spinning. Spectroscopy 2004;19(12):98–102.

Hu JZ, Wind RA, Rommereim DN. ^{1}H relaxation times of metabolites in biological samples obtained with non-destructive *ex vivo* slow-MAS NMR. Magn. Reson. Chem 2006;44:269–275. [PubMed: 16477679]

Hu, JZ.; Rommereim, DN.; Wind, RA.; Minard, K.; Sears, JA. A simple approach for obtaining high resolution, high sensitivity ^{1}H NMR metabolite spectra of biofluids with limited mass supply. In: Arabnia, HR.; Valafar, H., editors. Proceedings of The 2006 International Conference on Bioinfomatics and Computational Biology; CSREA Press; 2006. p. 360-366.

Jue, T. Bioenergetics implication of metabolic fluctuation during muscle contraction. In: Shulman, RG.; Rothman, DL., editors. Metabolomics by In Vivo NMR. John Wiley & Sonsw Ltd; England: 2005. p. 104-123.DL

Keshari KR, Zektzer AS, Swanson MG, Majumdar S, Lotz JC, Kurhanewicz J. Characterization of intervertebral disk degeneration by high-resolution magic angle spinning (HR-MAS) spectroscopy. Magn. Reson. Med 2005;53:519–527. [PubMed: 15723415]

Knaapen AM, Borm PJA, Albrecht C, Schins RPF. Inhaled particles and lung cancer. Part A: Mechanisms. Int. J. Cancer 2004;109:799–809. [PubMed: 15027112]

Kreis R. Quantitative localized ^{1}H MR spectroscopy for clinical use. J. Prog. Nucl. Magn. Reson. Spec 1997;31:155–195.

Li N, Sioutas C, Cho A, Schmitz D, Misra C, Sempf J, Wang M, Oberley T, Froines J, Nel A. Ultrafine particulate pollutants induce oxidative stress and mitochondrial damage. Environ. Health. Perspect 2003;111:455–460. [PubMed: 12676598]

Lindon JC, Nicholson JK, Holmes E, Everett JR. Metabonomics: Metabolic processes studies by NMR spectroscopy of biofluids. Concepts Magn. Reson 2000;12:289–320.

Lindon JC, Holmes E, Nicholson JK. Toxicological applications of magnetic resonance. Prog. Nucl. Magn. Reson. Spectr 2001;39:1–40.

Lindon JC, Holmes E, Nicholson JK. So what's the deal with metabonomics? Metabonomics measures the fingerprint of biochemical perturbations caused by disease, drugs, and toxins. Anal. Chem 2003;75:384A–391A.

Lindon JC, Holmes E, Nicholson JK. Toxicological applications of magnetic resonance. Prog. Nucl. Magn. Reson. Spectr 2004;45:109–143.

Mackinnon WB, Barry PA, Malycha PL, Gillett DL, Russell P, Lean CL, Doran ST, Barraclough BH, Bilous M, Moountford C. Fine-needle biopsy specimen of benign breast lesions distinguished from invasive cancer ex vivo with proton MR spectroscopy. Radiology 1997;204:661–666. [PubMed: 9280241]

Miller BE, Hook GE. Stimulation of surfactant phospholipid biosynthesis in the lungs of rats treated with silica. Biochem. J 1988;253:659–665. [PubMed: 2845927]

Millis KK, Maas WE, Cory DG, Singer S. Gradient, high-resolution, magic-angle spinning NMR spectroscopy of human adipocyte tissue. Magn. Reson. Med 1997;38:399–403. [PubMed: 9339440]

Mountford CE, Wright LC. Organization of lipids in the plasma membranes of malignant and stimulated cells: a new model. Trends Biochem. Sci 1988;13:172–177. [PubMed: 3255199]

Nelson, DL.; Cox, MM. Lehninger's Principles of Biochemistry. 4th Edition. W. H. Freeman and Company; New York: 2005.

Nicholson JK, Wilson ID. High resolution ^{1}H NMR spectroscopy of biological fluids. Prog. Nucl. Magn. Reson. Spectr 1989;21:449–501.

Nicholson JK, Lindon JC, Holmes E. ‘Metabonomics’: understanding the metabolic responses of living systems to pathophysiological stimuli *via* multivariate statistical analysis of biological NMR spectroscopic data. Xenobiotica 1999;29(11):1181–1189. [PubMed: 10598751]

O'Reilly KMA, Phipps RP, Thatcher TH, Graf BA, Van Kirk J, Sime PJ. Crystalline and amorphous silica differentially regulate the cyclo-oxygenase-prostaglandin pathway in pulmonary fibroblasts: Implications for pulmonary fibrosis. Am. J. Physio Lung Cell Mol. Physiol 2005;288(6):L1010.

Pollard, TD.; Earnshaw, WC. Cell Biology. Elsevier, Inc; 2004. p. 166

Porter DW, Millecchia L, Robinson VA, Hubbs A, Willard P, Pack D, Ramsey D, McLaurin J, Khan A, Landsittel D, Teass A, Castranova V. Enhanced nitric oxide and reactive oxygen species production and damage after inhalation of silica. Am. J. Physiol. Lung. Cell. Mol. Physiol 2002;283:L485–493. [PubMed: 12114212]

Reo NV. NMR-based metabolomics. Drug. and Chemical Toxicol 2002;25:375–382.

Ruiz-Cabello J, Cohen JS. Phospholipid metabolites as indicators of cancer cell function. NMR Biomed 1992;5:226–233. [PubMed: 1449961]

Schiller J, Naji L, Huster D, Kaufmann J, Arnold K. ^{1}H and ^{13}C HR-MAS NMR investigations on native and enzymatically digested bovine nasal cartilage. MAGMA 2001;13:19–27. [PubMed: 11410393]

Schins RPF. Mechanisms of genotoxicity of particles and fibres. Inhal. Toxicol 2002;14:57–78. [PubMed: 12122560]

Shen Y, Zhang R, Moore FJ, Kim J, Metz TO, Hixson KK, Zhao R, Livesay EA, Udseth HR, Smith RD. Automated 20 kpsi RPLC-MS and MS/MS with Chromatographic Peak Capacities of 1000-1500 and Capabilities in Proteomics and Metabolomics. Anal. Chem 2005;77:3090–3100. [PubMed: 15889897]

Shi X, Dalal NS, Hu XN, Vallyathan V. The chemical properties of silica particle surface in relation to silica-cell interaction. J. Toxicol. Environ. Health 1989;27:435–454. [PubMed: 2547978]

Shi X, Mao Y, Daniel LN, Saffiotti U, Dalal NS, Vallyathan V. Silica-induced DNA damage and lipid peroxidation. Environ. Health Perspect 1994;102(suppl. 10):149–154. [PubMed: 7705289]

Shi X, Mao Y, Daniel LN, Saffiotti U, Dalal NS, Vallyathan V. Generation of reactive oxygen species by quartz particles and its implication for cellular damage. Appl. Occup. Environ. Hyg 1995;10:1138–1144.

Shi X, Castranova V, Halliwell B, Vallyathan V. Reactive oxygen species and silica-induced carcinogenesis. J. Toxicol. Environ. Health, Part B: Crit Rev 1998;1:181–197.

Shukla A, Timblin C, BeruBe K, Gordon T, McKinney W, Driscoll K, Vacek P, Mossman BT. Inhaled particulate matter causes expression of nuclear factor (NF)-kappaB-related gene and oxidant-dependent NF-kappaB activation in vitro. Am. J Respir. Cell Mol. Biol 2000;23:182–187. [PubMed: 10919984]

Sime PJ, Xing Z, Graham FL, Csaky KG, Gauldie J. Adenovector-mediated gene transfer of active transforming growth factor-beta 1 induces prolonged severe fibrosis in rat lung. Journal of Clinical Investigation 1997;100(4):768–776. [PubMed: 9259574]

Sinha G. Trying to catch troublemakers with a metabolic profile. Science 2005;310:965–966. [PubMed: 16284158]

Smith RS, Smith TJ, Blieden TM, Phipps RP. Fibroblasts as sentinel cells. synthesis of chemokines and regulation of inflammation. Am. J. Pathol 1997;151:317–322. [PubMed: 9250144]

Spurney, RF.; Coffman, TM. The role of eicosanoids in transplant rejection. In: Ruffolo, RR., Jr.; Hollinger, MA., editors. Inflammation Mediators and Pathways. CRC Press Inc.; 1995. p. 129-145.

Steel, RGD.; Torrie, JH. Principles and procedures of statistics with special reference to the biological science. McGraw-Hill Book Company, Inc; New York: 1960.

Taylor JL, Wu CL, Cory D, Gonzalez RG, Bielecki A, Cheng LL. High-resolution magic angle spinning proton NMR analysis of human prostate tissue with slow spinning rates. Magn. Reson. Med 2003;50:627–632. [PubMed: 12939772]

Thrall RS, Peterson LB, Linehan JH, Abramoff P, Moore VL. The effect of immunization on the uptake of intratracheally administered antigen. Clin. Immunol. Immunopathol 1978;10:136–147. [PubMed: 668213]

Vallyathan V, Mega JF, Shi X, Dalal NS. Enhanced generation of free radicals from phagocytes induced by mineral dusts. Am. J. Respir. Cell Mol. Biol 1992;6:404–413. [PubMed: 1312851]

Vallyathan V, Shi X, Dalal N, Irr W, Castranova V. Generation of free radicals from freshly fractured silica dust: potential role in acute silica-induced lung injury. Am. Rev. Respir. Dis 1998:1213–1219.

Voelkel K, Krug HF, Diabate S. Formation of reactive oxygen species in rat epithelial cells upon simulation with fly ash. J. Biosci 2003;28:51–55. [PubMed: 12682424]

Ward, AG.; Courts, A. The Science and Technology of Gelatin. Academic Press; New York: 1977.

Waters NJ, Holmes E, Williams A, Waterfield CJ, Farrant RD, Nicholson JK. NMR and pattern recognition studies on the time-related metabolic effects of anaphthylisothiocyanate on liver, urine, and plasma in the rat: An integrative metabonomic approach. Chem. Res. Toxicol 2001;14:1401–1412. [PubMed: 11599932]

Weybright P, Millis K, Campbell N, Cory DG, Singer S. Gradient, high-resolution, magic angle spinning ^{1}H nuclear magnetic resonance spectroscopy of intact cells. Magn. Reson. Med 1998;39:337–345. [PubMed: 9498588]

Williams RE, Lenz EM, Lowden JS, Rantalainen M, Wilson ID. The metabonomics of aging and development in the rat: an investigation into the effect of age on the profile of endogenous metabolites in the urine of male rats using ^{1}H NMR and HPLC-TOF MS. Molecular BioSystems 2005;1:166–175. [PubMed: 16880980]

Wind RA, Hu JZ, Rommereim DN. High Resolution ^{1}H NMR Spectroscopy in Organs and Tissues Using Slow Magic Angle Spinning. Magn. Reson. Med 2001;46:213–218. [PubMed: 11477623]

Wind RA, Hu JZ, Rommereim DN. High-resolution ^{1}H NMR spectroscopy in a live mouse subjected to 1.5 Hz magic angle spinning. Magn. Reson. Med 2003;50:1113–1119. [PubMed: 14648558]

Wind RA, Hu JZ. Pandalai SG. Magnetic susceptibility effects in nuclear magnetic resonance spectroscopy of biological objects. Recent Res. Devel. Magnetism & Magnetic Mat 2003;1:147–169.

Wind, RA.; Hu, JZ. Method for high resolution magnetic resonance analysis using magic angle technique. US patents 665832 B2, 6670811, and 6836115 B2. 2003. 2004

Wind, RA.; Hu, JZ. Proton NMR in biological objects submitted to magic angle spinning. In: Worsfold, PJ.; Townshend, A.; Poole, CF., editors. Encyclopedia of Analytical Science, Second Edition. Vol. 6. Elsevier; Oxford: 2005. p. 333-342.

Wind RA, Hu JZ, Majors PD. Slow-MAS NMR: A new technology for in vivo metabolomic studies. Drug Discovery Today: Technologies 2005;2:291–294.

Wind, RA.; Hu, JZ.; Rommereim, DN. Advanced slow-magic angle spinning probe for magnetic resonsnce imaging and spectroscopy. US Patent 6653832 B2. 2006.

Wind RA, Hu JZ, Majors PD. Localized in vivo isotropic-anisotropic correlation ^{1}H NMR spectroscopy using ultraslow magic angle spinning. Magn. Reson. Med 2006;55:41–49. [PubMed: 16315205]

Wind RA, Hu JZ. In vivo and ex vivo high-resolution ^{1}H NMR in biological systems using low-speed magic angle spinning. Progr. Nucl. Magn. Reson. Spectr 2006;49:207–259.

Zhang K, Rekhter MD, Gordon D, Phan SH. Myofibroblasts and their role in lung collagen gene expression during pulmonary fibrosis. A combined immunohistochemical and in situ hybridization study. Am. J. Pathol 1994;145:114–125. [PubMed: 7518191]

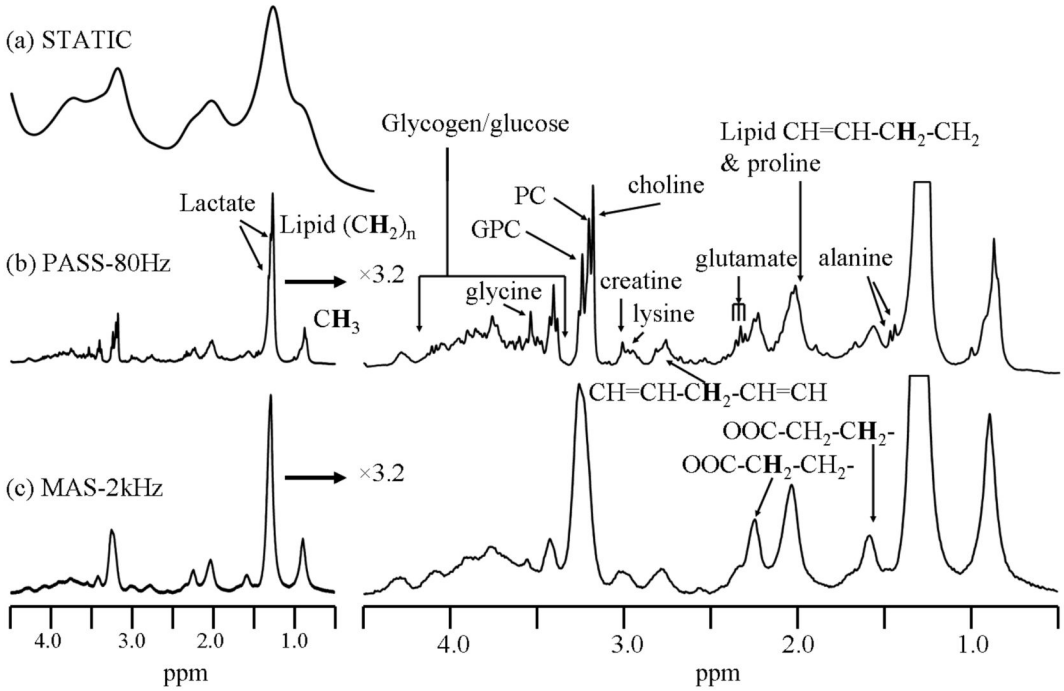

Figure 1.

The water suppressed ^{1}H NMR spectra obtained by the various techniques on a left lung lobe from a 7 days post silica exposed C57BL/6 mouse that was given a single silica dose of 5mg. (a) The static spectrum obtained by traditional NMR; (b) ^{1}H PASS spectrum obtained at 80Hz and (c) fast MAS ^{1}H NMR spectrum acquired at a sample spinning rate of 2kHz. The lung was first lavaged to obtain BALF prior to the experiment. The PASS spectrum was acquired using sixteen evolution increments and each evolution increment has 96 accumulations with a recycle delay time of 1s. The $\pi/2$ pulse width was 10 μs. The DANTE sequence used for water suppression contained 1000 pulses of pulse width of 0.8 μs and spaced by 100 μs. For details on performing PASS experiment, please consult reference (Wind et al 2001). Both the static (a) and the fast-MAS (b) spectra were acquired using the same amount of T_2 weighting as that of PASS using a standard CPMG pulse sequence with 128 accumulations, a recycle delay of 1s and the same water suppression sequence as used in PASS. Spectral assignments were made based on references (Bollard et al 2000, Garrod et al 2001).

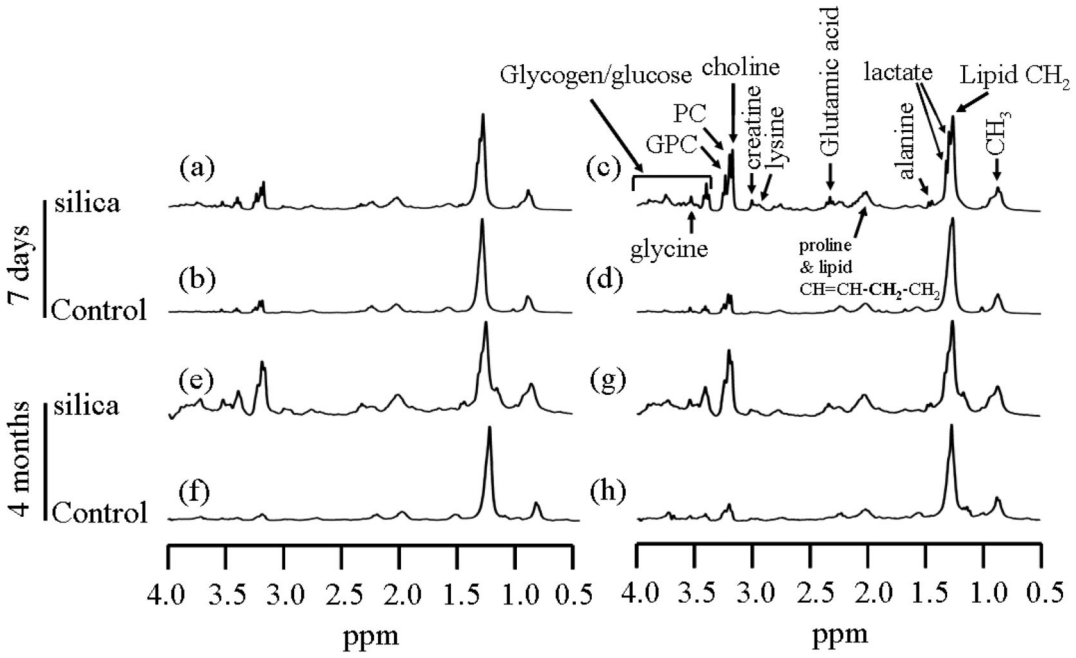

Figure 2.

^{1}H PASS spectra of excised left lungs of C57BL/6 mice 7 days and 4 months post treatment. (a), (c), (e) and (g) are from mice treated with 5mg silica dust/each mouse. (b), (d), (f) and (h) are from sham control mice instilled with saline. Mouse (a) and (b) were treated when they were 47days old while mice (c) and (d) were treated when they were 54 days old. In the plot, all the spectra are scaled in relation to the lipid CH_2 peak at about 1.28ppm. Each PASS spectrum was acquired using identical experimental parameters as those given in Figure 1. The weight of the lung used for each PASS experiment was between 30-80mg.

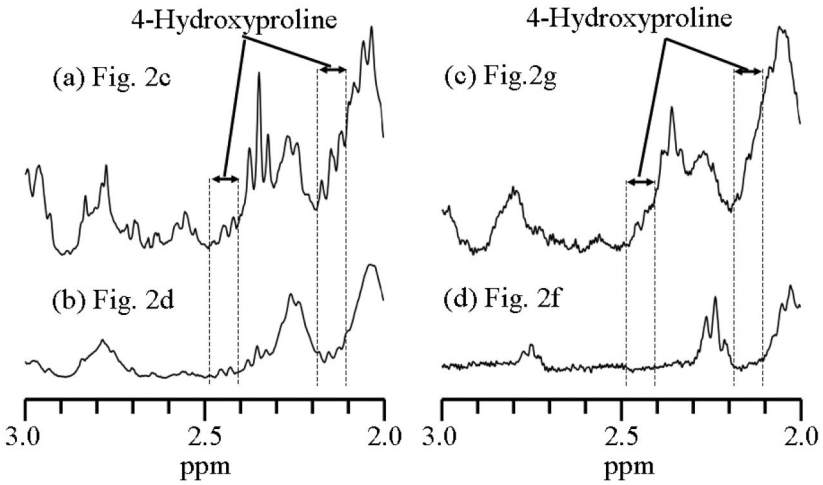

Figure 3.

The vertically expanded ^{1}H PASS spectra obtained from Figures 2c, 2d, 2g and 2f. As in Figure 2, the long chain lipid peak, $(CH_2)_n$ at about 1.28ppm, is scaled to the same height for all the spectra. 4-Hydroxyproline has ^{1}H NMR peaks (multiple peaks at each location) centered at about 2.14, 2.43, 3.45, 4.33 and 4.66 ppm, respectively. All of these peaks are overlapped with various other peaks of higher intensities. The spectral range between approximately 2.1 and 2.2 ppm was used as indicator for 4-Hydroxyproline in statistical analysis. It should be noticed that this assignment of 4-hydroxyproline can only be considered as a first order approximation. This is because there is a possibility that other peaks from unknown metabolites may also appear at the same spectral range.

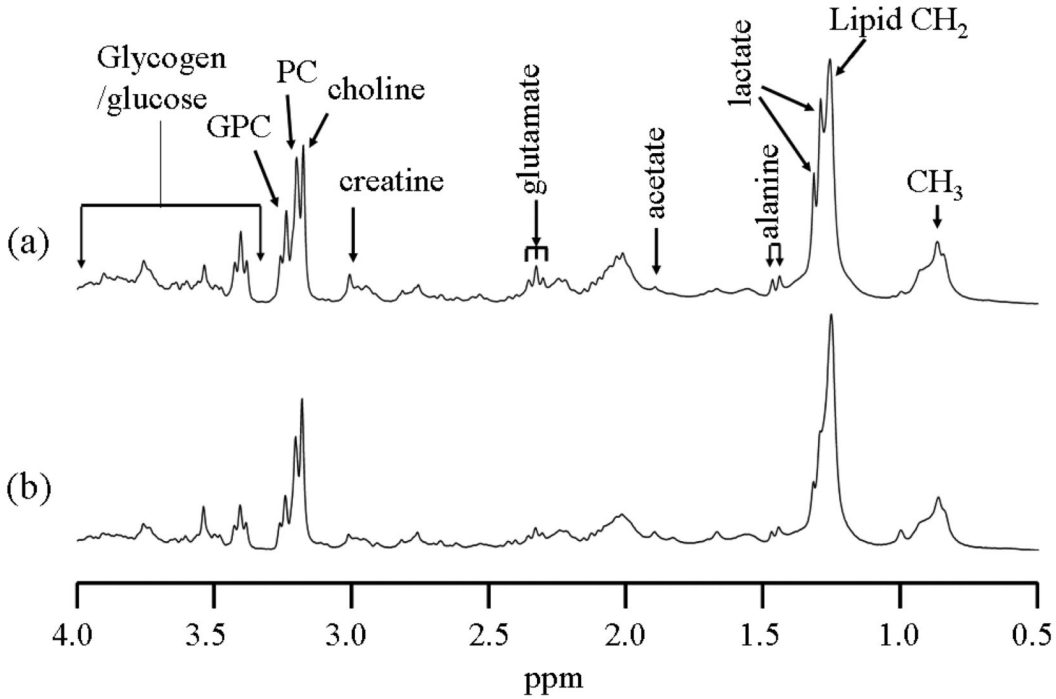

Figure 4.

^{1}H PASS spectra of excised in tact lung from mouse exposed to 5mg silica dust 7 days post exposure. The PASS spectra (a) and (b) correspond to two different locations that are detailed in the text.

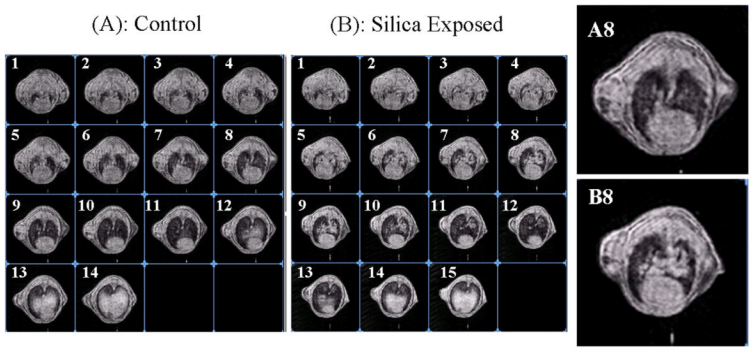

Figure 5.

Imaging slices of 85MHz 3D ^{1}H MRI of mice acquired in a magnetic field of 2T. (A) The control mouse that was instilled with saline; (B) Exposed counterpart that was instilled with 5mg silica dust. Both (A) and (B) were obtained 14 days after the intratracheal instillation. A8 and B8 are enlarged views for corresponding images in (A) and (B).

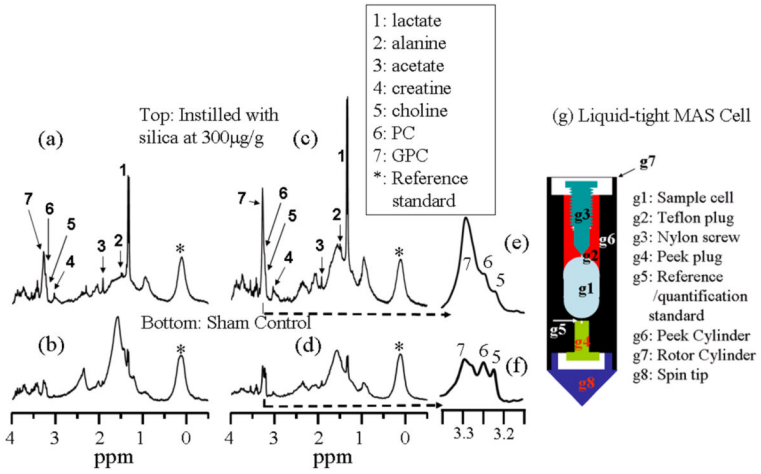

Figure 6.

Water suppressed 300MHz ^{1}H MAS (2kHz spinning rate) spectra of BALF fluids of both control and silica treated C57BL/6 mice. 80μl of BALF were used in each case. "*"indicates signals from the permanent external standard (i.e., the silica sealant labeled as "5" in Fig.6g). Mouse (a) and (b) were treated when they were 47days old while mouse (c) and (d) were treated when they were 54 days old. (a) and (c) are silica exposed mice while (b) and (d) are sham controls. (e) and (f) are expanded plots corresponding to the chemical shift regions containing choline, PC and GPC peaks in (c) and (d), respectively. Spectral assignments were made based on references (Bollard et al 2000,Garrod et al 2001).

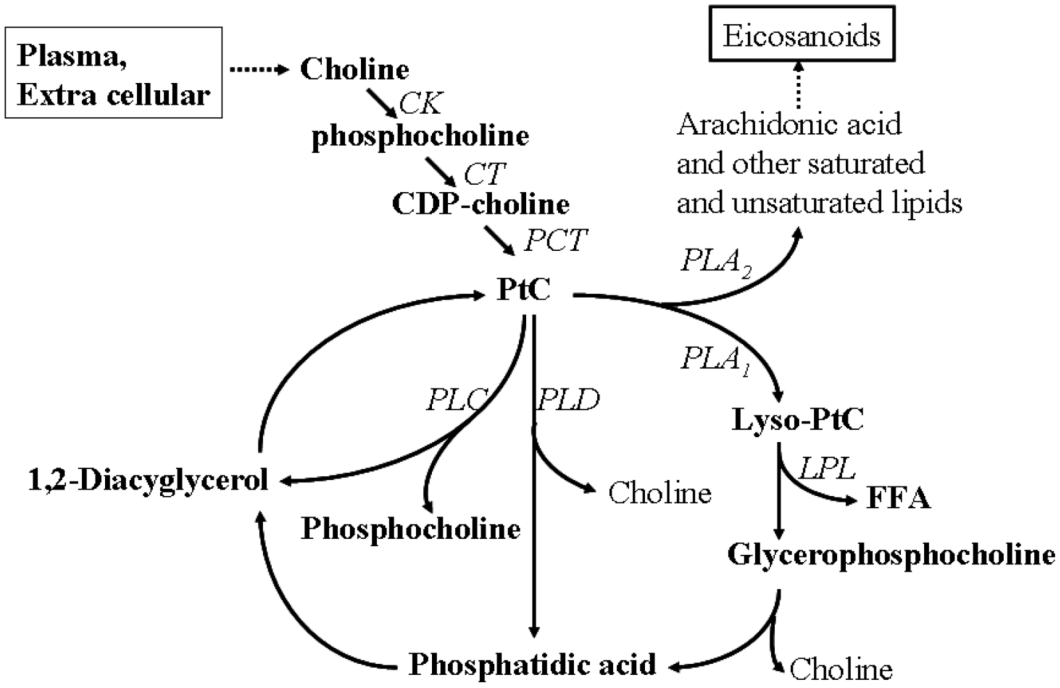

Figure 7.

Membrane choline phospholipids metabolism (MCPM), i.e., the biosynthesis and hydrolysis of phosphatidylcholine (PtC). Phosphorylation of choline to phosphocholine (PCho) by choline kinase (*CK*) is the first step in the biosynthesis of PtC. PCho is then converted to PtC via intermediates involving the rate-limiting enzyme CTP: phosphocholine cytidyltransferase (*CT*) and phosphocholine transferase (*PCT*). Hydrolysis of PtC is effected by three major PtC-specific enzymes, phospholipase C (*PLC*), phospholipase D (*PLD*), and phospholipase A_1 and A_2 (*PLA_1* and *PLA_2*). FFA, free fatty acid.

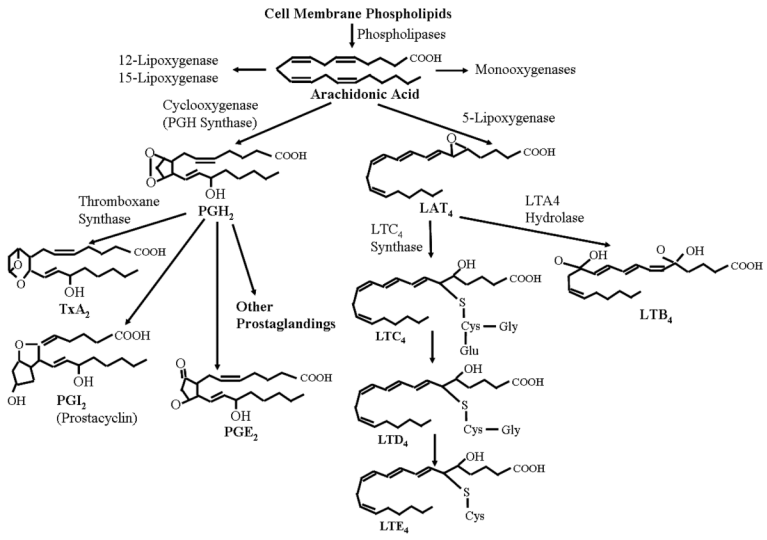

Figure 8.

Summary of arachidonic acid metabolism. After release from membrane phospholipids, arachidonate may be used as substrate by cycloxygenases, lipoxygenases, and P450-dependent monooxygenases. Metabolism of arachidonate by cycloxygenases produces prostaglandins and thromboxanes (TxA_2, PGI_2 and PGE_2), and metabolism by 5-lipoxygenase produces leukotrienes (LTA_4, LTB_4, LTC_4, LTD_4 and LTE_4). The effects of these labile compounds are exerted locally through interaction with specific cell surface receptors.

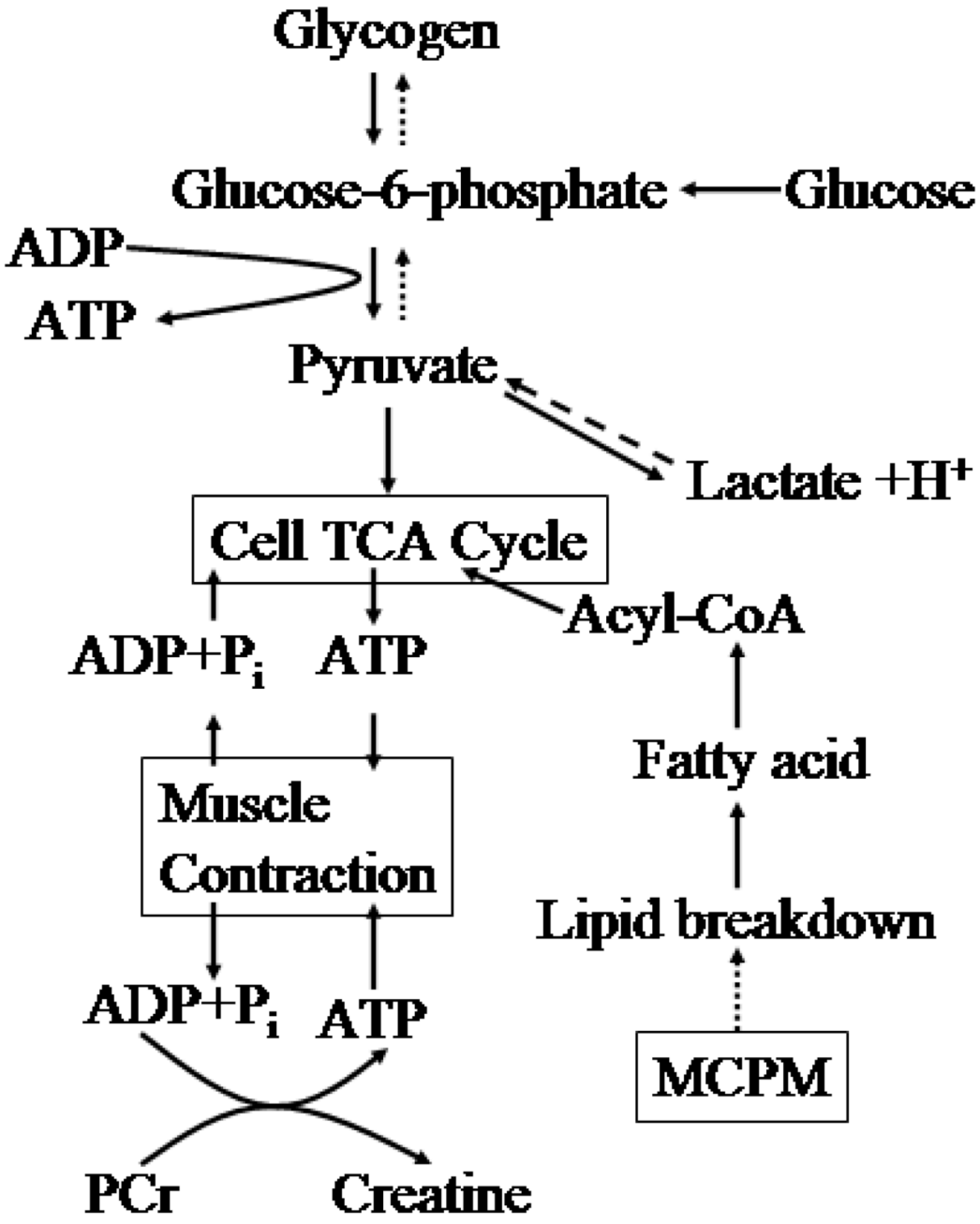

Figure 9.
Cellular energy pathway. A schematic drawing of the major metabolic pathways that control energy utilization. Based on our results on MCPM, we hypothesize that lipid breakdown is somehow linked to the MCPM pathway.

Table 1

Summary of the statistical analysis (Student's *t* test) for the ^{1}H PASS metabolite spectra of excised lungs from the silica exposed and control C57BL/6 mice 7-days and 4-months post exposure.

metabolite	mouse group	mean	Std of mean	*p
7-days post treatment				
CH_3	Silica	0.575	0.084	0.003
	Control	0.313	0.008	
Lactate	Silica	0.726	0.083	0.006
	control	0.339	0.141	
alanine	silica	0.150	0.060	0.017
	control	0.024	0.009	
proline & lipid CH=CH-C**H**$_2$-CH_2	silica	0.664	0.181	
	control	0.232	0.002	0.010
4-hydroxyproline	silica	0.18	0.068	0.024
	control	0.052	0.007	
Glutamic acid	silica	0.218	0.072	0.008
	control	0.037	0.008	
Lysine	silica	0.131	0.004	0.011
	control	0.03	0.007	
Creatine	silica	0.091	0.034	0.013
	control	0.014	0.0025	
Total choline	silica	0.786	0.265	0.011
	control	0.171	0.029	
Glycogen/glucose	silica	1.44	0.447	0.007
	control	0.268	0.044	
Glycine	silica	0.106	0.024	0.003
	control	0.025	0.007	
4-months post treatment				
CH_3	silica	0.334	0.064	0.267
	control	0.271	0.08	
4-hydroxyproline	silica	0.15	0.08	0.038
	control	0.04	0.02	
Total choline	silica	0.35	0.141	0.011
	control	0.084	0.039	
Glycogen/glucose	silica	0.516	0.293	0.030
	control	0.098	0.025	

* p indicates the probability of the null hypothesis, i.e., the means of the two normally and independently distributed populations are equal. For the 7-days post treatment groups, the sample sizes are n=4 for the silica exposed and n=3 for the control mice. For the 4-months post treatment, n=4 for both the silica exposed and the control groups.

Table 2

The relative peak intensities obtained from Figure 6.

	Spectrum	Peak Intensity							
		Standard	Lactate	Alanine	acetate	creatine	choline	PC	GPC
Silica	Fig.6a	1.0	2.43	0.09	0.33	0.14	0.39	0.71	1.06
	Fig.6c	1.0	3.83	0.06	0.25	0.29	0.76	1.23	2.47
control	Fig. 6b	1.0	0.44	0.03	0.07	0.04	0.19	0.29	0.34
	Fig. 6d	1.0	0.41	0.04	0.11	0.08	0.59	0.64	0.60

Note: Using the smaller value from Figs. 6a and 6c for the silica exposed mice and the larger value from Figs. 6b and 6d for the control mice, the concentration of lactate in the BALF of silica exposed mice is increased by at least 7.7 fold relative to the controls. Similarly, the concentrations of alanine, acetate, creatine and GPC are also increased by at least 0.5, 1.3, 0.75, and 0.77 fold, respectively.